Materials Science and Engineering A 524 (2009) 40–45

Contents lists available at ScienceDirect

Materials Science and Engineering A

journal homepage: www.elsevier.com/locate/msea

In situ Laue diffraction of metallic micropillars

R. Maaß, S. Van Petegem, C.N. Borca, H. Van Swygenhoven*

Paul Scherrer Institut, 5232 Villigen PSI, Switzerland

ARTICLE INFO

Article history:
Received 26 February 2009
Received in revised form 26 May 2009
Accepted 27 May 2009

Keywords:
Size effect
Micropillars
Micro-compression
Laue diffraction

ABSTRACT

Laue micro-diffraction performed on metallic micropillars prior to deformation revealed the presence of strain gradients and planar defects in samples made by focused ion beam (FIB) milling. In situ Laue micro-diffraction shows that such pre-existing gradients can play a role in the determination of the first activated slip system, and thus leading to un-expected geometrical strengthening. Lattice rotations resulting in the formation of substructures are observed at stresses well below the strength of the pillars usually defined as the stress at 5% strain.

1. Introduction

Size effects in plasticity resulting from the reduction in specimen size have received much attention in recent years since conventional theories do not explicitly incorporate geometrical length-scale dependencies. In order to circumvent the coupled effects of strain gradients, as are encountered in nano-indentation and wafer curvature testing, uni-axial micro-compression testing is a technique to study the effects of geometric size [1–4]. In these experiments pillars with diameters of the order of tens of microns down to 100 nm are compressed using a nano-indenter outfitted with a flat punch indenter. The results show a general trend of increasing strength with decreasing diameters. Rationale for such behavior is greatly debated, with emerging theories including dislocation exhaustion and stochastic, scale-free dislocation mechanisms [5–7]. Micropillars are typically fabricated using focused ion beam (FIB) machining from a thin film or bulk specimen. It is well-known that in metals FIB causes damage due to the Ga implantation [8]. It is often assumed that such damage is restricted to a small surface region and that the FIB procedure does not alter the mechanical properties [5,9,10], whereas other propose models for FIB induced hardening [11,12]. Computational simulations are currently being carried out in order to explore the origin of the observed geometric length scale size effect [13–15]. Up till now only macroscopic mechanical data and SEM observations are available as experimental input parameters for such simulations whereas very little is known about the evolving microstructure during compression. Furthermore it is assumed that the geometrical boundary conditions of the testing technique do not promote self-organization and multiplication of dislocations [5,16,17], which for example would lead to crystal rotation. To shed light on the initial microstructure and on possible FIB damage we have performed ex-situ Laue micro-diffraction on Si pillars made both by FIB milling and by deep reactive ion etching. We furthermore present an in situ time resolved Laue micro-diffraction experiment that captures the changes in microstructure during deformation of Au micropillars [18]. The dynamics of the Laue patterns show that the initial strengthening seen in the smaller pillars can be explained by plasticity starting on a slip system that is geometrically not predicted but selected because of the character of pre-existing strain gradients within the sample. Moreover as the plasticity proceeds, significant rotation of the crystal is observed, which implies strain hardening that is also suggested by the evolving peak topologies.

2. Experimental setup

The presented experiments were done with a custom designed in situ micro-compression device (MCD) [18] at the MicroXAS beam line of the Swiss Light Source (SLS) (see Fig. 1a). Micro-compression and white beam micro-focused X-ray diffraction are combined to probe the microstructure as a function of deformation strain. Force and displacement are measured with a single axis 1D Triboscope transducer from Hysitron Inc. The positioning of the flat punch compression tip above the sample is performed with the help of two high resolution optical microscopes positioned in two orthogonal view axes that are perpendicular to the compression axis. A smooth touchdown procedure is carried out by a sub-nm resolution piezo stage that stops the approach once a given transducer displacement

* Corresponding author. Tel.: +41 56 310 2931; fax: +41 56 310 3131.
E-mail address: helena.vs@psi.ch (H. Van Swygenhoven).

0921-5093/$ – see front matter © 2009 Elsevier B.V. All rights reserved.
doi:10.1016/j.msea.2009.05.062

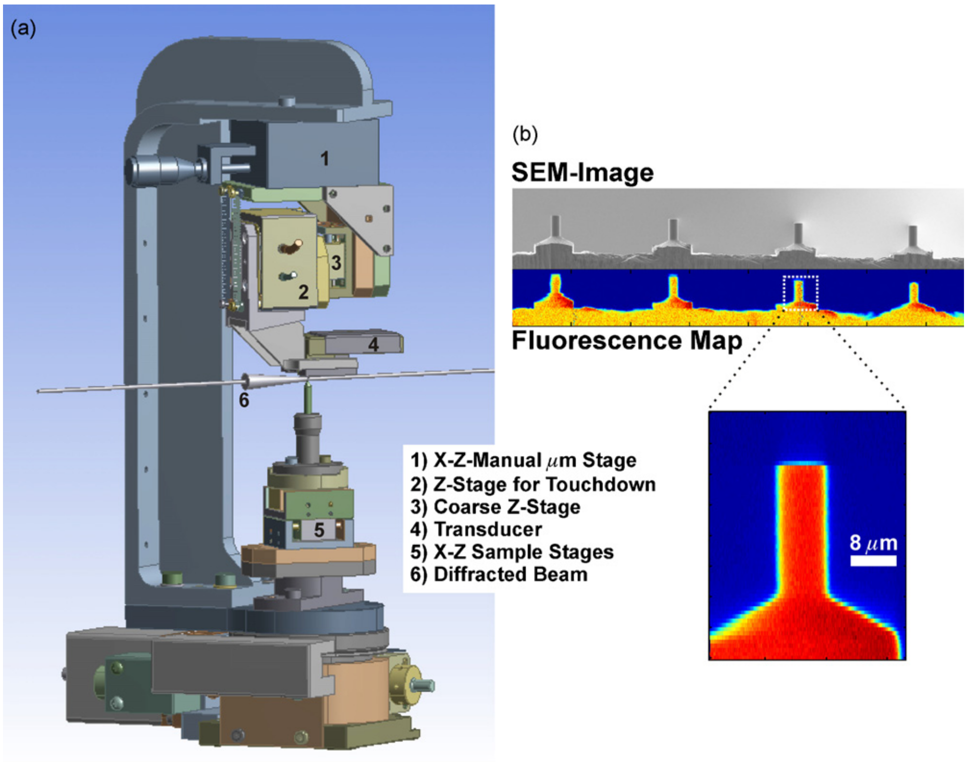

Fig. 1. (a) Schematic of the in situ micro-compression device (MCD), (b) four 8 μm metallic micropillars imaged by scanning electron microscopy (SEM) and by X-ray fluorescence. The inset shows the fluorescence signal from one pillar which was scanned with a step size of 300 nm.

threshold is attained. The results presented here are obtained in a load controlled mode with loading rates of 1–3 μN/s and a single crystal diamond flat punch tip with an end diameter of 22 μm. The samples were illuminated in transmission geometry with a polychromatic X-ray beam with an energy distribution ranging from 2 to 22 keV. The X-ray beam is focused with a set of Kirckpatrik–Baez mirrors, yielding a beam size of typically 0.8–2 μm in the focal plane and an angular divergence of 0.2 mrad. The samples are positioned with sub-micron precision in the X-ray beam using an X-ray fluorescence detector. This is demonstrated in Fig. 1b, which presents a row of Ni micropillars with a diameter of 8 μm visualized with X-ray fluorescence in comparison with a conventional scanning electron microscopy (SEM) image. The inset of Fig. 1b demonstrates the high precision that can be achieved using this technique. Diffracted X-rays are recorded on a two-dimensional Photonic Science FDI-VHR 150 charged coupled device (CCD) with a pixel size of 31 μm. The detector parameters such as tilt and sample-to-detector distance are calibrated using a least-square refinement of a Laue pattern from a strain-free single crystal Si wafer. The angular width of Si diffraction spots is about 0.06°, which is a good measure for the experimental resolution of the complete setup. Recorded Laue patterns were indexed using the triplet method, as described by Tamura et al. [19]. This allows determining the crystallographic orientation of the probed volume with high accuracy. During in situ testing the diffraction peaks evidence peak asymmetries, collective peak movements and peak splitting. Peak asymmetries are due to lattice curvatures; e.g. strain gradients and provide therefore information about the perfection of the single crystal. Statistically stored dislocations (SSD) results in symmetric peak broadening; an initial content of geometrically necessary dislocations (GND) cause a lattice curvature resulting in peak streaking [20]. Peak streaking is evidenced by an asymmetric peak shape that has a maximum (major) and minimum (minor) peak width. Collective changes in peak positions are a signature of lattice rotations. A peak split is a signature of a plastically bent portion of the crystal, which has broken up into smaller disoriented sub-volumes that each diffract with slightly different angles. The misorientation angle can easily be calculated from the Laue peaks and the diffraction geometry.

This paper reports first on examples of initial defects found in focused ion beam (FIB) machined micropillars, followed by a section that relates the pre-existing defects to the plastic response. Finally an example is given of a micropillar with no significant initial defects. It is shown that such a pillar in general deforms according to the slip system with the highest critically resolved shear stress.

3. Results

3.1. Pre-existing defects in micropillars

Single crystal Si micropillars (1 and 2.7 μm) having a ⟨0 0 1⟩-orientation were either produced by FIB (2.7 μm) or by a special etching technique (1 μm) [21]. Final Ga^+ currents of 50 pA where used to prepare the FIB-synthesized samples. Using Pt markers below the Si pillars the samples could be located. The Laue patterns of the Si pillars show mainly reflections from the {3 3 1}, {1 1 3} and {2 4 2}-families of lattice planes for an incoming beam parallel to a ⟨0 1 1⟩-direction. Fig. 2 summarizes the results for the Si pillars. For the etched pillar a Laue pattern with an inset of the SEM image (a) is shown together with a truncated contour plot (b) and a 3D intensity profile (c) of the (1 −3 3)-reflection. All reflections of the etched pillar show peak shapes similar to the peak profiles of a Si wafer reference sample. For the FIB-Si pillar an SEM picture (d) and the contour plots of the (1 −3 3) (e) and the (1 3 3)-reflection (f) are shown together with a 3D profile of the (1 −3 3)-peak (g). Laue spot streaking was observed for all recorded reflections of the FIB-prepared pillar. The derived streaking direction can be interpreted

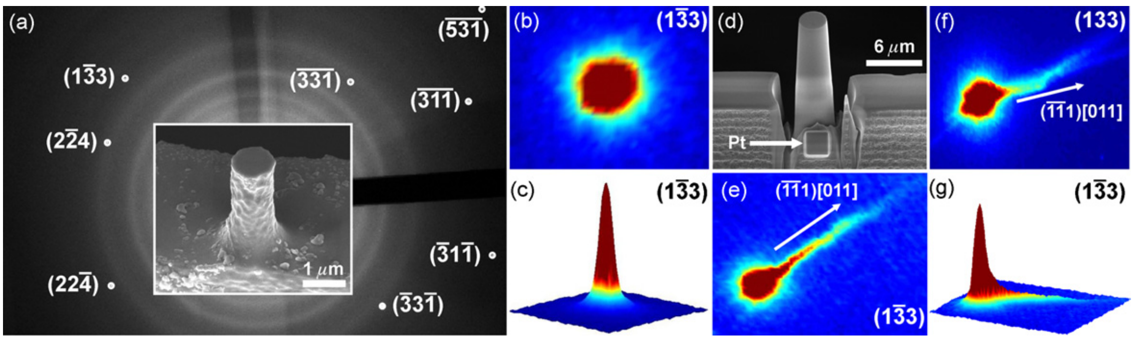

Fig. 2. (a) Laue pattern and SEM image of the etched Si micropillar, with the (1 −3 3) Laue spot shown both as a contour plot (b) and as intensity profile (c). For the FIB-Si pillar an SEM image (d) is shown, two contour plots of a (1 −3 3) and (1 3 3) Laue spot (e and f) evidencing streaking according to GNDs on the (−1 −1 1)[0 0 1] slip system, and an intensity profile of the streaked (1 −3 3)-reflection (g).

as an excess dislocation content on the (−1 −1 1)[0 0 1] slip system, clearly demonstrating the introduction of strain gradients caused by the FIB sputtering technique.

Besides initial strain gradients apparently introduced by FIB procedure, some of the investigated metal pillars evidence the presence of at least two crystallographic orientations prior to loading. Fig. 3 shows the Laue analysis of a 1 and an 8 μm Ni⟨1 2 3⟩-micropillar prior to deformation. Each Laue spot of the Laue pattern from the 1 μm pillar is split into two peaks as shown in Fig. 3a for the (2 −2 −2) reflection. One peak corresponds to the same crystallographic orientation as the sample substrate, whereas the second peak deviates 0.55° from this orientation. When illuminating the upper part of the pillar the intensity of the second peak strongly increases, indicating the presence of a misfit boundary at the base of the pillar. A similar finding has been reported for an 800 nm Au pillar [22]. Scanning the 8 μm Ni pillar shows the presence of a misfit that extends from the bottom at the left hand side to a height of ca. 10 μm at the right hand side, as shown in Fig. 3b, where the red frames indicate the locations where split peaks are observed. The splitting distance at position 2 correspond with a 0.07° misorientation, which in a first approximation [23] corresponds with a GND density of 4.9×10^{12} m^{-2}. More examples of initial defects found in the initial microstructure of FIB pillars can be found in [21,22,24].

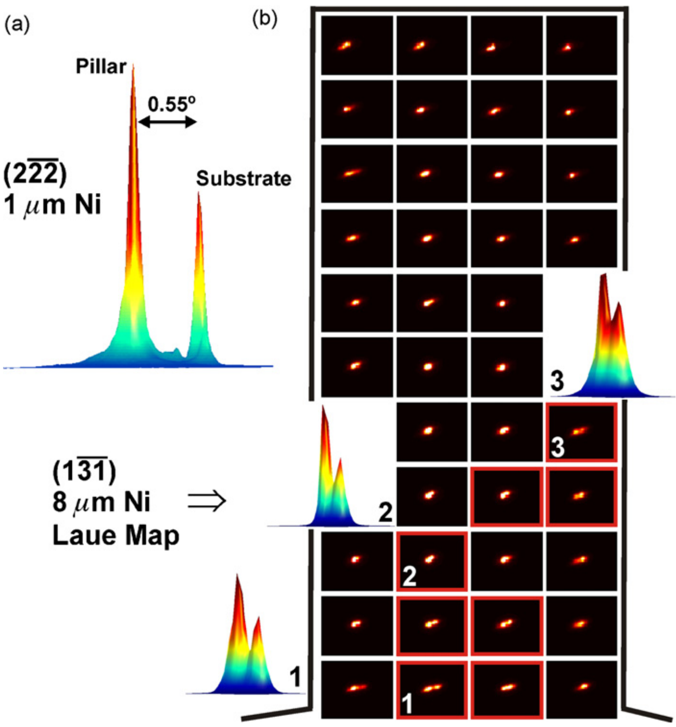

Fig. 3. (a) A (2 −2 −2)-reflection from an as-prepared 1 μm Ni pillar showing a 0.55° misfit between the pillar and the substrate, (b) a spatial Laue map of a (1 −3 −1)-reflection over an 8 μm Ni pillar, where the red framed spots are split as is displayed for three positions.

3.2. *In situ Laue micro-compression of a 2 μm Au pillar*

A 2 μm Au⟨3 4 6⟩-micropillar with an aspect ratio of 1.9 was compressed during Laue diffraction. Fig. 4 shows the stress–strain curve together with the SEM image after compression to 25%. The numbers indicated on the curve give the corresponding Laue pattern. The deformation curve is characterized by an initial steep increase of the stress, followed by rapid strain bursts. Post-mortem SEM investigation shows slip traces according to the (1 −1 1), the (1 −1 −1) and the (−1 −1 1) slip planes (inset Fig. 4). The white beam diffraction pattern recorded prior to deformation contains five Laue spots of high intensity, namely the (−2 0 0), (0 2 −2), (−3 1 −1), (−1 −3 1) and (−2 2 −2)-reflection. All Laue spots of the undeformed pillar show continuous streaking demonstrating the presence of a strain gradient. Fitting the reflections with a 2D Pearson VII profile, result in a major/minor peak width ratio of (8.6 pixel)/(2.4 pixel) and (9.3 pixel/2.0 pixel) for the (−2 0 0) and (−1 −3 1) Laue spot, respectively. The full width at half maximum (FWHM) in the radial θ-direction amounts 0.23° for the (−2 0 0)-reflection.

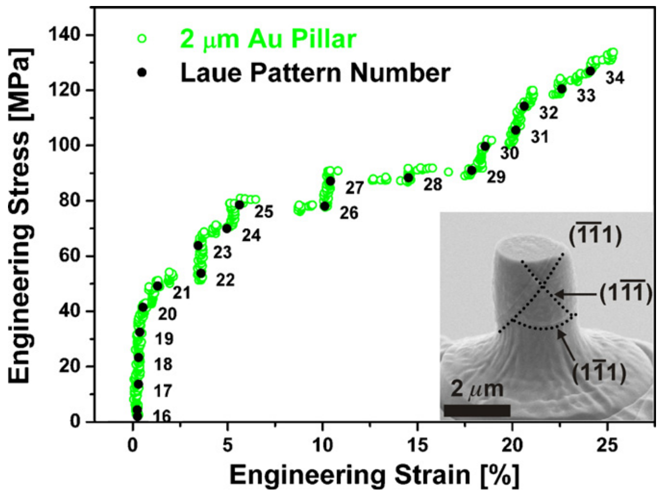

Fig. 4. The stress–strain curve of the 2 μm Au⟨3 4 6⟩-micropillar, the numbers indicate the recorded Laue patterns. An inset shows the SEM-image of the deformed sample, with the three observed slip planes indicated.

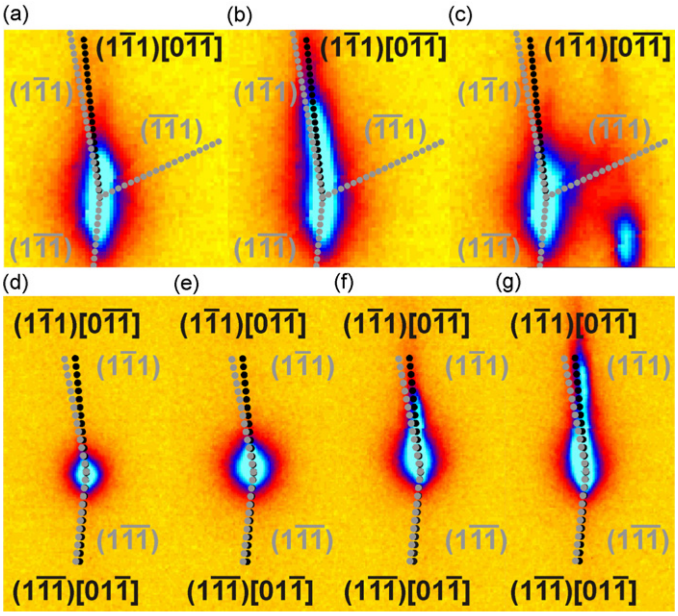

Fig. 5. (a–c) Streaking of the (−2 2 −2)-peak from the 2 μm pillar at 0, 40 and 77 MPa, respectively demonstrating the maximum gradient at 40 MPa and a gradient relief in connection with a peak splitting (boundary formation), (d–g) streaking of the (−2 2 −2)-peak from the 10 μm pillar for the unloaded state (d), at 12 MPa (e), at 30 MPa (f) and at 35 MPa (g) indicating a minor initial strain gradient and an isotropic broadening at 2.3% strain (e). Black lines are rotation directions, grey line are streaking directions.

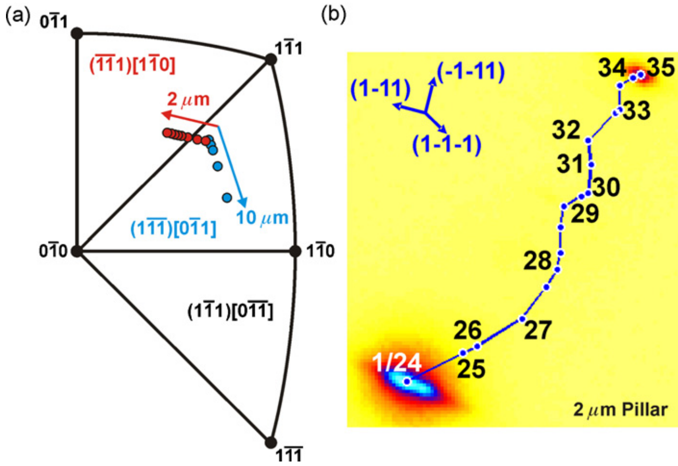

Fig. 6. (a) Stereographic projection of the vertical crystal axis for the 2 μm (red) and 10 μm (blue) pillar, (b) the initial intensity distribution of the (−2 0 0) Laue spot (Laue pattern 1), and the final position of (−2 0 0) satellite (Laue pattern 35) together with the intermediate path indicated by numbers on the stress strain curve. (For interpretation of the references to color in this figure legend, the reader is referred to the web version of the article.)

During the initial stages of loading where the stress raises very steeply, all reflections evidence an increasing amount of streaking. During the first strain bursts the peak sharpens again, and a satellite peak is formed. Upon continued loading, this satellite peak moves in discrete steps along different directions further away from the original peak.

Fig. 5a–c shows the intensity distribution of the (−2 2 −2)-reflection from the 2 μm Au pillar prior to deformation (a), at 40 MPa when maximum streaking is achieved corresponding to number 20 on the flow curve (b) and at 77 MPa when the satellite is formed corresponding with number 25 (c). On these plots, the streaking directions (grey lines) are shown for particular slip systems. Also shown (in black) are the directions the Laue peak should move according to classical crystal rotation associated with slip on the particular slip systems (a direction perpendicular to the load axis and the normal to the slip plane). Applying this type of analysis to all indexed peaks, it has to be concluded that the streaking can be assigned to the presence of unpaired dislocations with a Burgers vector [0 −1 −1] lying in the (1 −1 1) slip plane. At the moment of the burst (Laue pattern 20) streaking of the Laue spot reduces in amount, is however still present. When the applied load reaches a value of 77 MPa another large strain burst is observed coinciding with the take off of the satellite peak (Laue pattern 25). The direction the satellite takes off is situated in between the directions to be expected for slip along (1 −1−1)[0 −1 1] and slip along (−1 −1 1)[1 −1 0], indicating that at this strain the two other slip systems are already operating. Between the first strain burst and the formation of the satellite peak, the Laue streaking reduces further and the final width of the mother peak is narrower compared to the width prior to loading, demonstrating a partial strain gradient relief in the pillar.

The paths of all satellite diffraction peaks during deformation uniquely define the rotation of the crystal. Fig. 6a shows, using an inverse pole plot of the primary triangle formed by the [0 −1 0], [1 −1 0] and the [1 −1 1] poles, the rotation of the vertical crystal axis of the 2 μm Au pillar (in red) plotted in a stereographic projection. The geometrically predicted slip systems are shown for the primary and neighbouring triangles. For uniaxial constraint compression geometries, the vertical axis is expected to rotate towards the [0 −1 0]–[1 −1 0]-line using the (1 −1 −1)[0 1 −1] slip system, after which the (1 −1 1)[0 −1 −1] system will be equally activated maintaining the orientation along the [0 −1 0]–[1 −1 0]-line. However in the case of this 2 μm pillar, the crystal rotates in the opposite direction, continuing towards the line [0 −1 0]–[0 −1 1] after having crossed the [0 −1 0]–[1 −1 1]-line. From the path of the satellite peak, the different rotation directions can be derived. For instance, the bursts between 28–29 and 30–32 can be assigned to the (−1 −1 1)[1 −1 0] slip system, whilst the 29–30 and 32–33 bursts clearly evidence the intermittent activity of the (1 −1 −1)[0 −1 −1] system. The 2 μm pillar seems to deforms predominantly using the geometrically unpredicted harder (−1 −1 1) slip plane. Note that as the crystal rotates the critical resolved shear stress changes and accordingly the Schmid factors also change.

3.3. In situ Laue micro-compression of a 10 μm Au pillar

A larger 10 μm micropillar Au⟨3 4 6⟩-pillar made of the same material as the 2 μm pillar and having an aspect ratio of 1.3 was also deformed in situ. In contrast with the smaller pillar, no significant initial strain gradients could be observed as supported by Pearson 2D-VII fitting, which gave a peak with ratio of (3.6 pixel)/(1.9 pixel) for the (−2 0 0)-peak. The angular width of the (−2 0 0) Laue spot is 0.1°, which also is clearly lower compared to the 2 μm sample. The sample was compressed to 20% strain with two loading cycles, of which only the first one is displayed in Fig. 7a. Again the numbers along the curve indicate when the Laue patterns were recorded. After deformation well distributed (1 −1 −1) slip lines are found all over the pillar and some (1 −1 1) slip lines are seen at one side close to the pillar base (inset Fig. 7a). The rotation of the vertical axis of the 10 μm pillar is shown in the inverse pole figure (Fig. 6a, blue data points) demonstrating that the pillar deforms on the geometrically predicted (1 −1 −1)[0 1 −1] slip system resulting in crystal rotation where the vertical axis rotates towards the [0 −1 0]–[1 −1 0]-line.

Fig. 5d–g shows the (−2 2 −2)-reflection prior to deformation (d), at 12 MPa corresponding with Laue pattern 40 (e), at 30 MPa corresponding with Laue pattern 90 (f) and at 35 MPa corresponding with Laue pattern 105 (g). Despite the initial anisotropic peak shape, first isotropic peak broadening is observed till 12 MPa

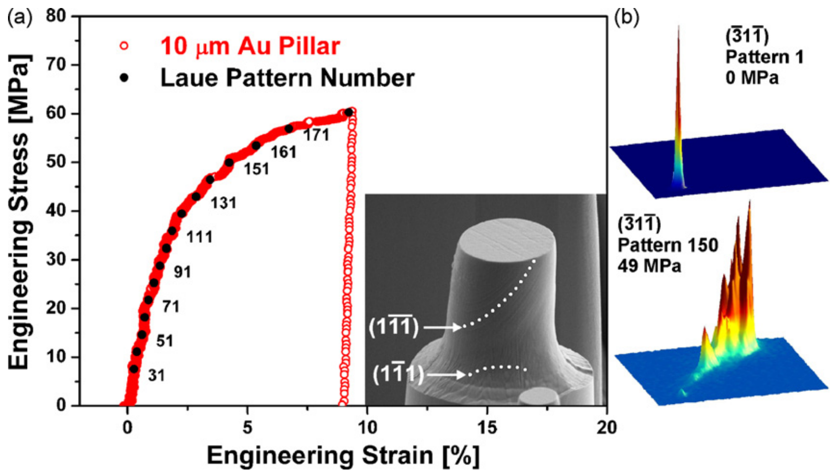

Fig. 7. First part of the flow curve of a 10 μm Au pillar with every 20th Laue pattern indicated along the curve. The inset shows the compressed sample after the full 20% deformation, depicting predominantly (1 −1 −1) well distributed slip lines and a few (1 −1 1) slip line at the base of the sample (b) shows (−3 1 −1)-reflection at 0 and 49 MPa evidencing substructure formation in the probed volume of the pillar depicted in the inset of (a).

(pattern 40), followed by a directional streaking reaching a maximum at 30 MPa (pattern 105). Despite the presence of the small initial strain gradient, the Laue spot splits into sub-peaks moving away along the classically predicted (1 −1 −1) rotation direction, with a remaining low intensity part along the (1 −1 1) rotation direction, conform to the slip lines visible in the SEM surface of the pillar. Fig. 7b compares the (−3 1 −1)-reflection prior to loading and at 49 MPa (pattern 150) indicating substructure evolution that results in strain hardening. Note that the (1 −1 1)[0 −1 −1]-system is the next favoured slip system predicted classically when the compression axis approaches the borders of the primary triangle.

4. Discussion

The Laue experiments address three important issues affecting the outcome of a micro-compression experiment: (a) the presence of pre-existing defect structures in single crystal pillars, (b) the influence a pre-existing strain gradient can have on the onset of plasticity and (c) the boundary conditions of the test.

Any sub-volume taken from a well annealed single crystal will contain a certain SSD density depending on the quality of the bulk sample. The presence of streaked and split Laue spots shows that as-prepared metallic micropillars often exhibit strain gradients (hence GNDs) or low-angle boundaries. The origin of these defects are a matter of debate. The comparison of the FIB prepared and etched Si pillars clearly illustrates that the FIB introduces damage in the Si. The relatively low intensity Laue streaking observed for the FIB-Si pillar could be related to a small volume of material that is damaged by FIB milling. A similar comparison for metallic micropillars is not possible due to the lack of data on metallic pillars that are not produced using FIB preparation techniques. Recent work by Bei and Shim demonstrated that FIB milling introduces damage that increases the surface hardness [12]. The vast amount of lattice defects revealed by in situ Laue measurements are certainly contributing to the large scatter observed for the flow stress of pillars of identical sizes [3,9,16]. A similar conclusion was drawn from compression experiments performed on pre-deformed Mo pillars containing a certain amount of dislocations. These experiments show that the initial dislocation content does not only reduce the flow stress relative to the defect free crystal, but also induces a large scatter in the measured values [25].

In contrast to the presence of pre-existing defects, little is known about their influence on the initial deformation behavior. In situ Laue diffraction performed on 2 μm diameter Au pillars synthesized using FIB demonstrates that plasticity starts on a hard slip system that is geometrically not predicted, but seems to be selected because of the character of the pre-existing strain gradient. The larger 10 μm sample made from the same Au foil had an inferior strain gradient and in this pillar plastic deformation did not start on a geometrically hard slip system but on the classical predicted one. These results suggest a geometrical strengthening effect of pre-existing strain gradients, something that can be only studied in depth by using in situ diffraction techniques.

Micro-compression is often referred to as being a uniaxial test with an un-constrained geometry [2,5] that minimizes imposed deformation gradients [16,17,26]. In situ Laue experiments have shown that compression of micropillars results in building up of GNDs, followed by the formation of substructures and large lattice rotations and this already at relative low strains. To demonstrate the enhanced strength as a function of pillar diameter, the flow stress at a relative large strain (5% [2] or 10% [9]) is usually used. The Laue experiments demonstrate however that crystal rotation occurs already at much lower strains, as also was observed for in the in situ Laue compression of Cu micropillars [27]. Early lattice rotation implies that a strain hardening mechanisms will be active.

Acknowledgements

The authors thank T. Lehnert, M.D. Uchic, and C.A. Volkert for the preparation of the Si, Ni, and Au samples. For beam line support gratitude is expressed towards D. Grolimund and M. Willimann from the MicroXAS beam line of the Swiss Light Source (SLS). S. Brandstetter and J. Zimmermann are thanked for helping out with the measurements. Furthermore the authors thank Hysitron Inc. for technical support during the implementation of the in situ MCD. HVS thanks the Swiss National Science Foundation (No. SNF-2100-065152.01, SNF-200020-116283/1) and the European Commission (6th framework) for financial support of the project NANOMESO.

References

[1] M.D. Uchic, D.M. Dimiduk, J.N. Florando, W.D. Nix, Science 305 (2004) 986.
[2] C.A. Volkert, E.T. Lilleodden, Philos. Mag. 86 (2006) 5567.
[3] C.P. Frick, B.G. Clark, S. Orso, A.S. Schneider, E. Arzt, Mater. Sci. Eng. A 489 (2008) 319.
[4] D. Kiener, C. Motz, T. Schoberl, M. Jenko, G. Dehm, Adv. Eng. Mater. 8 (2006) 1119.
[5] J.R. Greer, W.C. Oliver, W.D. Nix, Acta Mater. 53 (2005) 1821–1830.
[6] S.I. Rao, D.M. Dimiduk, T.A. Parthasarathy, M.D. Uchic, M. Tang, C. Woodward, Acta Mater. 56 (2008) 3245.
[7] D.M. Dimiduk, C. Woodward, R. LeSar, M.D. Uchic, Science 312 (2006) 1188.

[8] C.R. Hutchinson, R.E. Hackenberg, G.J. Shiflet, Ultramicroscopy 94 (2003) 37.
[9] J.R. Greer, W.D. Nix, Phys. Rev. B (2006) 73.
[10] Z.W. Shan, R.K. Mishra, S.A.S. Asif, O.L. Warren, A.M. Minor, Nat. Mater. 7 (2008) 115.
[11] D. Kiener, C. Motz, M. Rester, M. Jenko, G. Dehm, Mater. Sci. Eng. A-Struct. 459 (2007) 262.
[12] H. Bei, S. Shim, Appl. Phys. Lett. 91 (2007) 111915.
[13] V.S. Deshpande, A. Needleman, E. Van der Giessen, J. Mech. Phys. Solids 53 (2005) 2661.
[14] D. Weygand, M. Poignant, P. Gumbsch, O. Kraft, Mater. Sci. Eng. A 483/484 (2008) 188.
[15] C.R. Weinberger, W. Cai, Proc. Natl. Acad. Sci. U.S.A. 105 (2008) 14304.
[16] D.M. Dimiduk, M.D. Uchic, T.A. Parthasarathy, Acta Mater. 53 (2005) 4065.
[17] A.S. Budiman, S.M. Han, J.R. Greer, N. Tamura, J.R. Patel, W.D. Nix, Acta Mater. 56 (2008) 602.
[18] R. Maass, S. Van Petegem, H. Van Swygenhoven, P.M. Derlet, C.A. Volkert, D. Grolimund, Phys. Rev. Lett. 99 (2007) 145505.
[19] N. Tamura, A.A. MacDowell, R. Spolenak, B.C. Valek, J.C. Bravman, W.L. Brown, R.S. Celestre, H.A. Padmore, B.W. Batterman, J.R. Patel, J. Synchrot. Radiat. 10 (2003) 137.
[20] G.E. Ice, R.I. Barabash, in: F.R.N. Nabarro, J.P. Hirth (Eds.), Dislocation in Solids, vol. 13, Elsevier, 2007, Chapter 79.
[21] R. Maass, D. Grolimund, S. Van Petegem, M. Willimann, M. Jensen, H. Van Swygenhoven, T. Lehnert, M.A.M. Gijs, C.A. Volkert, E.T. Lilleodden, R. Schwaiger, Appl. Phys. Lett. 89 (2006) 151905.
[22] R. Maass, S. Van Petegem, J. Zimmermann, C.N. Borca, H. Van Swygenhoven, Scr. Mater. 59 (2008) 471.
[23] R.I. Barabash, G.E. Ice, F.J. Walker, J. Appl. Phys. 93 (2003) 1457.
[24] R. Maass, S. Van Petegem, D. Grolimund, H. Van Swygenhoven, M.D. Uchic, Appl. Phys. Lett. 91 (2007) 131909.
[25] H. Bei, S. Shim, G.M. Pharr, E.P. George, Acta Mater. 56 (2008) 4762.
[26] W.D. Nix, J.R. Greer, G. Feng, E.T. Lilleodden, Thin Solid Films 515 (2007) 3152.
[27] R. Maass, S. Van Petegem, D. Grolimund, H. Van Swygenhoven, D. Kiener, G. Dehm, Appl. Phys. Lett. 92 (2008) 071905.